Robust Multidimensional Optical Modulation Based on Hybrid Subcarrier/Amplitude/Phase/Dual Polarization for Wavelength-Division Multiplexing Systems

Andres Ortega, *aortega@ups.edu.ec* and Brayan Peñafiel, *bpenafiel@ups.edu.ec*

***Abstract*—Here, we propose a novel scheme based on advanced techniques of digital modulation in optical communications to achieve a single-channel transmission rate above 100 Gb/s. We utilize a hybrid scheme amplitude/phase/frequency/dual polarization, combined with multidimensional dual lattice and a low-density parity-check-coded modulation. The Stokes parameters are applied to the proposed scheme to map the four-dimensional classical polarization I_X, Q_X, I_Y, Q_Y in a three-dimensional space. In addition, in the proposed system, the packing theory is applied to the bit interleaver process, three wavelengths are packaged before being transmitted over a wavelength-division multiplexing optical channel. This modulation process is carried out using symmetrical geometric shapes, such as a hypercube or a polyhedron, based on the molecular links theory using a grouping of 12 and 13/15 bits for the cubic and spherical lattices, respectively. The proposed technique is evaluated in the context of long distance communications over distances up to 100 km. The bit error rate results showed that the optical signal-to-noise ratio was approximately 4 dB over a distance of 50 km.**

In addition, the power spectral efficiency was found to be 3 lambda, which is considered good performance considering the effects of distance and the non-linear effects influencing the number of lambdas. Also, we use an optical time division multiplexing scheme (OTDM) in order to achieve a transmission rate beyond 1Tbit/s, where the speed effect is evaluated, taking into consideration that the power spectral efficiency is degraded.

Furthermore, the average noise floor is -60dBm for all transmission distances. These findings are expected to contribute to the future implementation of robust long-distance optical communication infrastructure.

***Index Terms*—Coherent Optical CommunicationsPolyhedronHypercubeMultidimensional ModulationsStokes parametersPoincaré sphere**

I. Introduction

In recent years, network operators have been considering and installing network infrastructures even more robust than those before them. The rapidly increasing demand for transmission capacity and the ineffective use of optical fiber links have led to many studies to develop advanced schemes that achieve transmission rate beyond 240 Gb/s per wavelength channel.

A promising approach to improving the transmission performance of future access networks, called multidimensional modulations was discovered a long time ago by Wei [1]. This technique involves the use of a rectangular or cross-lattice grouping technique to provide other modulations formats. This strategy improves the spectral efficiency (SE) to a level that approaches the Shannon limit.

This technique has more recently been applied to modern mobile access networks, such as sparse code multiple access networks (SCMA) [2] to achieve the high capacity needed to support large volumes of information and massive connectivity.

It is widely known, that optical-fiber communication is a strong candidate for connecting the backbone with the end users in future access networks. For this reason, research has been done to optimize optical channels by using advanced modulation formats so that they can transmit data at higher rates with flexible spectral and power efficiency. Furthermore, N-dimensional signal constellations may be incorporated to increase the system performance compared to that using traditional two-dimensional (2D) formats.

In coherent detected optical transmission, polarization-division-multiplexing (POLMUX) can be used to generate two orthogonal polarization signals, X and Y, for transmission through a single-wavelength channel with a high SE and ultra-high speed [3]. In this context, passive optical networks with two orthogonally polarized orthogonal frequency-division multiple access signals have recently been proposed. This system can transmit data at a rate of 108 Gb/s and with an excellent bit error rate (BER) of $1.4x10^{-3}$ over a transmission distance of 20 km by standard single-mode fiber transmission with a 1:32 optical split [4].

Adaptive turbo-trellis-coded modulation (ATTCM32QAM) enables communication at a rate near the Shannon limit with a $7.3dB$ coding gain compared to an uncoded system and offers a low BER of $BER = 1x10^{-3}$ [5]. In this way, wavelength-division multiplexing (WDM) can facilitate the realization of elastic optical networks and flexible transceivers.

Another promising technology is the polarization switching system, which sends a three-dimensional (3D) constellation with an asynchronous in-phase/quadrature (IQ) polarization, which represents the transmitted symbol in 3D [6]. Dual-polarization (DP) modulation provides a lower SE but better performance for a long distance transmission [7].

4D set-partitioning quadrature amplitude modulation (SP-QAM) is a special case of advanced optical modulation, in which a regular 4D cubic can be constructed by polarization-division multiplexing (PDM). A PDM-QAM model using a

A. Ortega and B. Peñafiel is with the Research Group in Telecommunications GITEL, Universidad Politecnica Salesiana, Cuenca, Ecuador.

coherent detection scheme with Reed-Solomon encoding was shown to improve the SE and provide a data transmission rate over 112 Gb/s [8]. In another study, the use of 4D 512-ary and 2048-ary SP-QAM signals and soft-decision forward error correction (FEC) with penalties resulted in BERs of $3.8x10^{-3}$ and $2x10^{-2}$ respectively [9].

In addition to the use spectrally-efficient modulation formats low-density parity-check (LDPC) codes can be incorporated into the physical design for new schemes to make them compatible with 4D modulations and, thereby, enable coherent optical communications with high aggregate bit rates. LDPC codes offer significant benefits compared to other codes and hybrid codes like turbo-trellis code modulations. In this context, 4D bit-interleaved LDPC-coded modulation has been developed by connecting a distributed-feedback (DFB) laser to a polarization beam splitter (PBS) to combine two polarization (X and Y) for each IQ modulator, thus, forming the structure of a 4D modulator [10]. The aggregate information bit rates with 16-, 32- and 64-QAM were measured as 160, 200, and 240 Gb/s, respectively; the best optical SNR of approximately 5 dB and a BER of $1x10^{-8}$ was attained with 16-QAM. In another study, 320 Gb/s data transmission was achieved using an M-ary 3D constellation with LDPC coded modulation; an SNR of nearly 12 dB and a BER of $1x10^{-9}$ was achieved for 8-QAM [6].

Therefore, the optimization of the power efficiency of an N-dimensional constellation that provides both flexible SE and high power efficiency at the same time can be solved by considering it as a sphere-packing problem [11]. The number of degrees of freedom for optical transmission can be represented by the vertical axis, where the first and second dimensions represent the electrical field of the X-polarized IQ components, and the third and fourth dimensions represent the electrical field electrical of the Y-polarized IQ components. In this context, a 4D lattice is constructed, and optimized with respect to the discrete time represented by the horizontal axis. This approach has been used to optimize a 3D constellation with four degrees of freedom, achieving data transmission of 224 Gb/s over a distance of 100 Km.

The use of polarization-mode dispersion can improve the coding gain due to error floor and the iterative exchange of extrinsic soft-bit reliabilities between *a posterior probability*. Hussam developed a way to implement such a modulation with different sub-carriers in a 3D space using coded hybrid sub-carrier/amplitude/phase/polarization (H-SAPP) [12]. Using Stokes parameters, H-SAPP allows 20 points to be incorporated into a 3D constellation mapping in the form of a dodecahedron inscribed in a Poincaré sphere based on regular polyhedrons [13]. Numerical results using 20-HSAPP show that $BER = 1x10^{-6}$ with an OSNR of $0.5dB$ could be achieved with a back-to-back configuration.

Here, we propose a hybrid subcarrier/amplitude/phase/dual polarization (H-SAPDP) system for an optical transmission of $300Gb/s$. To improve the performance, the system is based on polyhedrons. We demonstrate that the proposed system can be significantly banked to the Shannon limit over optical channels of different distances using WDM techniques.

The use of multidimensional modulations is a novel technique that holds promise for future generations of communication systems with both enhanced SE and superior BER performance. The SE and BER performance are known to be inversely proportional to one another according to the Shannon theory. In addition, the system may suffer from distortion effects if larger amounts of information are transmitted. However, the use of multidimensional techniques mitigates these challenges because, if the amount of information increases, it can be packaged by an interleaving bit distribution process to generate an N-dimensional lattice. This approach reduces the bit error rate, the inter-symbol interference, and the power transmission and consequently increases the SE as if two different modulations were being used at the same time: high-index modulation to improve the SE and low-index modulation to enhance the BER performance.

The proposed technique is implemented with different lattice dimensions in the interleaver process: a hypercubic multidimensional lattice with 16 symbols for 12 bits in an even alignment, and a polyhedron-spherical lattice with 32 symbols for 13 or 15 bits in an odd alignment. 12_13 or 15 bits are allocated to each block and packed with three sub-carriers composed of DP signals (I_X, Q_X, I_Y, Q_Y) and aligned in parallel (i.e., they transmit at the same time). One bit is added to denote the change from even to odd alignment; thus, the packed block will have 5 bits and, consequently, the distribution packing can be set in the range of 13_15 bits.

Finally, this packaging is transformed into a 4D optical signal using Jones vectors and Pauli matrices designed according to the parameters of the polarized signal. Thus, the H-SAPDP system performs dual-lattice packing with multidimensional modulations at 50 GS/s. In this way, the binary input is divided among the 4D carriers for transmission over a distance of 50, 80, or 100 km. This approach is compared with dodecahedral techniques based on the Poincaré technique and with different-dimensional packing.

Several possible constructions for the packing lattice have been proposed; however, unfortunately, this remains an unsolved problem in mathematics. The face-centered cubic lattice is obtained using a generator matrix in which the vectors represent the deep holes that arise from sphere packing (referred to as glue vectors). Another strategy is to consider the kissing number, which represents how many spheres can be arranged so that they all touch one central sphere of the same size [14]. In this study, we base the lattice on the theory of the sphere-packing problem which can be observed in the orange pyramid in fruit stands. Using this lattice configuration, the advantage of the triangles found in pyramids lead to geometrically equivalent packings.

To be precise, herein, we define the thickness (also called *density*, *sparsity* or coverage) as the number of spheres that contain a single point in space.

The remainder of this paper is organized as follows. Section II presents a description of the optical system considered here and the H-SAPDP coded modulation including the lattice packing (Section II-A), the dual lattice used to build the cubic and spherical lattices (Section II-B), the interleaver process (SectionII-C), the multidimensional modulator (Section II-D), and Stokes and polarized signal parameters (Section II-E). The

numerical results of the simulation are presented in Section III. Finally, the conclusions are summarized in Section IV.

II. H-SAPDP Coded Modulation

There are many ways of building a constellation lattice in order to optimize the signal constellations using N-dimensions. Fig.1 shows different methods of polarization over an optical fiber. Previously, 4D formats with single polarization and switch polarization were severely limited due to the synchronization of X and Y signals (Fig.1(b) and Fig.1(c)) [15]. Today, it is possible to modulate different signals with orthogonal X and Y polarization with total dependency between them. Thus, we leveraged the four dimensions of the optical carrier field as shown in Fig.1(d) in order to transport 16-point rectangular constellations and 28-point circular constellations through a cube and hypercube respectively in the 3D with total independence among them.

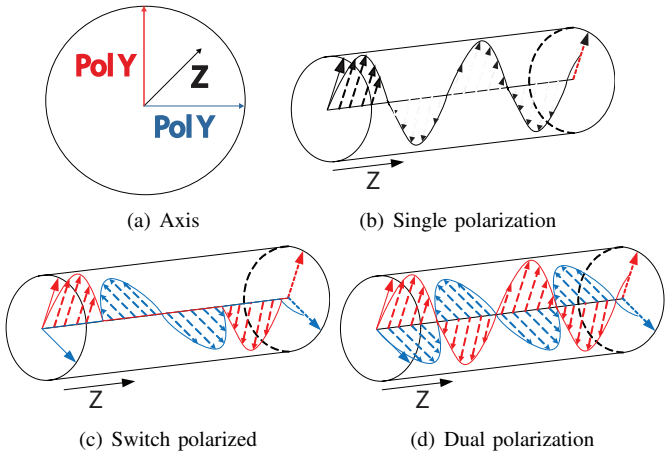

(a) Axis (b) Single polarization

(c) Switch polarized (d) Dual polarization

Fig. 1. Optical wave polarization techniques.

The proposed system, shown in Fig.II is composed of m-bit sources of n bits. Each source inserts input bit streams to the H-SAPDP transmitter to obtain a 4D lattice for each sub-carrier, $A\lambda_q$. These carriers transmit modulated optical pulses to achieve different constellations, as shown in Fig.7 (i.e., a cubic or spherical lattice, which are described later; Fig.8). All the carriers are combined and transmitted by a single-mode optical fiber. Finally, at the receiver end, an optical splitter divides the optical carriers to recover the information. Fig.3(a) shows the general block diagram of the H-SAPDP transmitter which accepts m-bit inputs from the information sources, passes them through a set of identical LDPC encoders with a code rate of $R = k/n$, where k represents the number of information bits that the encoder accepts and n the length of the resulting codeword. The encoded data from these branches is forwarded to an $[m \times n]$ block interleaver where it is written row-wise and read column-wise. In addition, the interleaver process performed by a dual-lattice multidimensional $[D_N \times D_N]$ building matrix that is defined based on the lattice-packing process.

A. *Lattice Packing*

We use the molecular-links theory to solve one of the famous open problems in mathematics called *sphere packing*, where the goal is to determine how densely a large number of identical spheres can be packed together. It is known that spheres do not fit well together; there is always some wasted space between them, called **deep holes**, as shown in Fig.4. In the dense packing of equally sized spheres in N-dimensional space (real numbers), a sphere in $\mathbf{R^N}$ with center $u = (u_1, \ldots, u_N)$ and radius ρ contains of all the points $x = (x_1, \ldots, x_N)$ such that:

$$(x_1 - u_1)^2 + (x_2 - u_2)^2 + \ldots + (x_N - u_N)^2 = \rho^2 \quad (1)$$

In the packed lattice, there are spheres with centers $u + v$ and $u - v$. Thus, the coordinates forming the basis of the lattice are defined by the glue vectors:

$$\begin{aligned} v_1 &= (v_{11}, v_{12}, \ldots, v_{1m}) \\ v_2 &= (v_{21}, v_{22}, \ldots, v_{2m}) \\ &\cdots \\ v_N &= (v_{N1}, v_{N2}, \ldots, v_{Nm}) \end{aligned} \quad (2)$$

where $m > N$. The *generator matrix* of the N-dimensional lattice can be described follows:

$$M = \begin{bmatrix} v_{11} & v_{12} & \cdots & v_{1m} \\ v_{21} & v_{22} & \cdots & v_{2m} \\ \vdots & \vdots & \cdots & \vdots \\ v_{N1} & v_{N2} & \cdots & v_{Nm} \end{bmatrix} \quad (3)$$

Let the determinant of Λ be equal to the determinant of matrix A, with is called the *Gram matrix* for the lattice and is defined as $A = MM'$. Now we can define the density, Δ, of a lattice packing as the proportion of the space that is occupied by the spheres. Thus, the density of a periodic packing is given by $\Delta = s \times V_s / (\det \Lambda)^{1/2}$, where s is the number of spheres, and V_s is the volume of each sphere.

B. *Dual Lattice* D_N^*

The checkerboard lattice is defined as $D_N = \{(\mathrm{x}_1, \cdots, \mathrm{x}_N) \in \mathbf{Z}^N : \mathrm{x}_1 + \cdots + x_N\}$ and is obtained by coloring the points of $\mathbf{Z}^N$ in an alternating pattern. $\mathbf{Z}$ is the set of integer points on a line segment (i.e., a one-dimmensional lattice) as marked on the Coxeter-Dynkin diagram [14]. If $N \geq 4$, then, the glue vectors that are part of the generator matrix M are defined as follows:

$$\begin{aligned} [0] &= (1, 0, 0, 0) \\ [1] &= (0, 1, 0, 0) \\ [2] &= (0, 0, 1, 0) \\ [3] &= (1/2, 1/2, 1/2, 1/2) \end{aligned} \quad (4)$$

The elements of the last glue vector are equal to one-half because that the packing radius is normalized at $\rho = 1/2$. Hence,

$$D_N^* = D_N \cup ([1] + D_N) \cup ([2] + D_N) \cup ([3] + D_N) \quad (5)$$

and

$$M = \begin{bmatrix} 1 & 0 & \cdots & 0 & 0 \\ 0 & 1 & \cdots & 0 & 0 \\ \vdots & \vdots & \ldots & \vdots & \vdots \\ 0 & 0 & \cdots & 1 & 0 \\ \frac{1}{2} & \frac{1}{2} & \cdots & \frac{1}{2} & \frac{1}{2} \end{bmatrix} \quad (6)$$

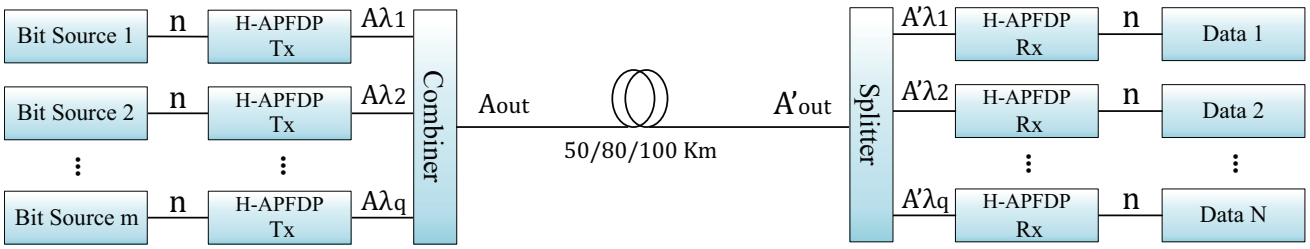

Fig. 2. Block Diagram Multi-Dimensional optical system

C. *Interleaver Process*

The information that is output by the encoder is grouped into different N-dimensional lattices to obtain M and, subsequently, form the output bitstream m. However, we propose packaging strategies with 12, 13, and 15 bits. In this way, different types of multidimensional dual-lattice packing,with different signal polarization parameters are used to obtain different signal constellations (Fig.7 and Fig.8). The signal polarization parameters based on the Stokes theory are described in the next section.

Fig.5 shows the interleaver bit distributions for 12, 13 and 15 bits, which are evaluated in terms of performance and compared with previous results presented by Hussam in [12] to optimize the interleaver. 4D multidimensional packages of 16 symbols can be transmitted independently using four Stokes parameters as well as quadrature phase-shift keying (Q-PSK) and IQ modulation, each with both polarizations (X and Y) as shown in Table.I. To package 12 bits in an even alignment with a 4D constellations (Fig.7) shows for each sub-carrier, λ_q, the bits are packaged in 12 dimensions, $D_N^* \times D_N^*$, where the rows are written based on the glue vector of M, forming the block shown in Fig.5(a).

For the 13 bit odd alignment, we use 32 symbols per sub-carrier to form the polyhedral and hypercubic multidimensional constellations (Fig. 8). The first column shows the odd bits, which are defined according to the most significant bit. These are used to decide whether to use the 16 symbols shown in Table.I or the remaining 16 symbols shown in Table.II. To maintain consistency in the data interleaving, the first dimension of the packing must contain $bit1$ for every sub-carrier as shown in Fig. 5(b).

Similarly, for 15 bits in an odd alignment, 32 symbols are used for each sub-carrier. However, the interleaver bit distribution is packaging 5 bits inside each sub-carrier to obtain the block shown in Fig 5(c).

D. *Multidimensional Modulator*

The symbol-mapping process is defined based on X-Y polarization information according to the lookup tables (LUTs) presented in Tables I and II to generate a 4D cube or polyhedron, respectively, as described in [16].

The $I_{X_{\lambda_q}}/Q_{X_{\lambda_q}}$ and $I_{Y_{\lambda_q}}/Q_{Y_{\lambda_q}}$ driving signals in the mapper output pass through the zero-insertion training symbols process defined as eight times the q-carrier frequencies (i.e., $\left(\widehat{I}_{X_{\lambda_q}}\right)$), before being combined with the optical pulses generated by the mode-locked fiber laser (MLFL) [17] using periodic rectangular pulses $A_0(t) = \sum_{n=-\infty}^{\infty} \prod_n (t - T_m) \cdot e^{j\omega_{\lambda_q} \cdot n \cdot t}$, where n is the number of infinite pulses, $T_m = 1/f_m$ where f_m is frequency of the modulator at 50 GHz [18]. The complex degree of coherence (ϕ) within A_X regarding the A_Y component, describes the orientation at the X-Y plane, this angle also is called the azimuth [19]. The azimuth for a completely polarized signal appears when $\phi = n\pi$ $(n = \pm 1; \pm 2; \pm 3; ...)$, hence ϕ is independent of time [20]. Therefore, the LUT maps each set of m bits onto quadruple driving signals using Stokes parameters (shown below) in order to obtain a modulated pulse, $A_X \lambda_q$ [21], where λ_q depends on the even versus odd alignment in the frequency domain, as shown in Fig. 5.

Then, the signal is divided by an optical splitter with the corresponding wavelength, which is generally defined as follows:

$$A_{0\lambda_q}(t) = A_0 \cdot e^{j\left(\phi_{X/Y}(t) + \omega_{\lambda_q}(t)\right)} \tag{7}$$

ϕ_X and ϕ_Y are the orientation of the polarizer, which are both corrupted by the same phase noise of the transmitter.

Once the optical signal is input to PBS, it is branched for the X and Y polarization to obtain the instantaneous amplitudes of the two orthogonal vectors both modulated by IQ-MZM [22]. The in-phase and quadrature components are described in Equations 8 and 9 respectively:

$$\begin{aligned} A_{0\lambda_q, I_{X/Y}}(t) &= \frac{-|A_0|}{2} Sin\left(\phi_{X/Y}(t)\right) \cdot e^{j\omega_{\lambda_q}(t)} \\ A_{0\lambda_q, Q_{X/Y}}(t) &= \frac{-|A_0|}{2} Sin\left(\phi_{X/Y}(t)\right) \cdot e^{j\omega_{\lambda_q}(t)} \end{aligned} \tag{8}$$

$$\begin{aligned} \phi_{I_{X/Y}}(t) &= \frac{\hat{I}_{X/Y_{\lambda_q}}(t) \cdot \pi \cdot Cos(2\pi \cdot f_m \cdot t)}{2V_\pi} \\ \phi_{Q_{X/Y}}(t) &= \frac{\hat{Q}_{X/Y_{\lambda_q}}(t) \cdot \pi \cdot Cos(2\pi \cdot f_m \cdot t)}{2V_\pi} \end{aligned} \tag{9}$$

where V_π is the voltage to reach a phase shift. Thus, the modulated pulses for X and Y polarization are represented as follows:

$$\begin{aligned} A_X(t) &= \mathfrak{Re}\left\{A_{0\lambda_q, I_X}\right\} + \mathfrak{Im}\left\{A_{0\lambda_q, Q_X}\right\} \\ A_Y(t) &= \mathfrak{Re}\left\{A_{0\lambda_q, I_Y}\right\} + \mathfrak{Im}\left\{A_{0\lambda_q, Q_Y}\right\} \end{aligned} \tag{10}$$

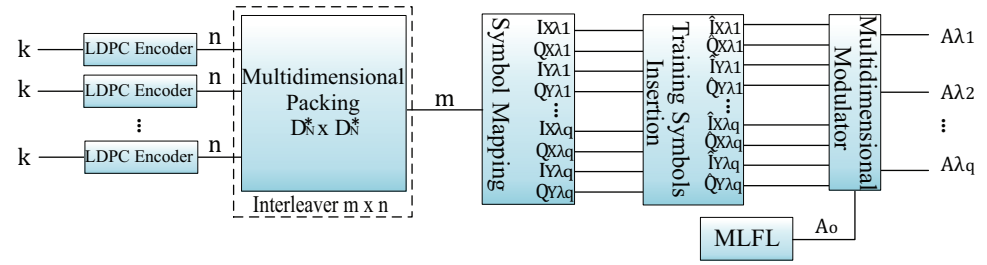

(a) H-SAPDP Transmitter Scheme

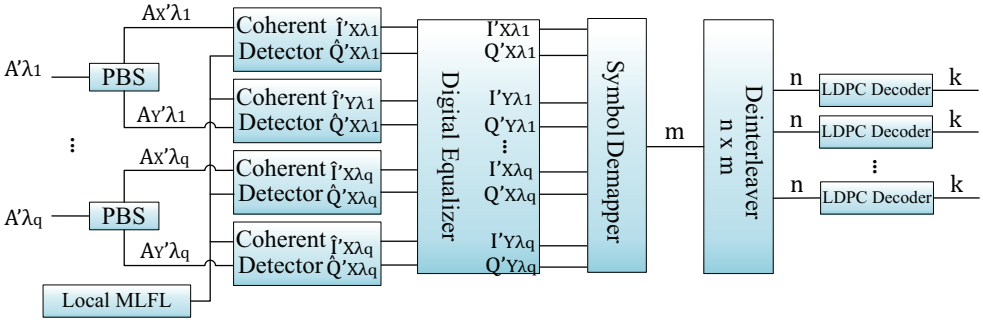

(b) H-SAPDP Receiver Scheme

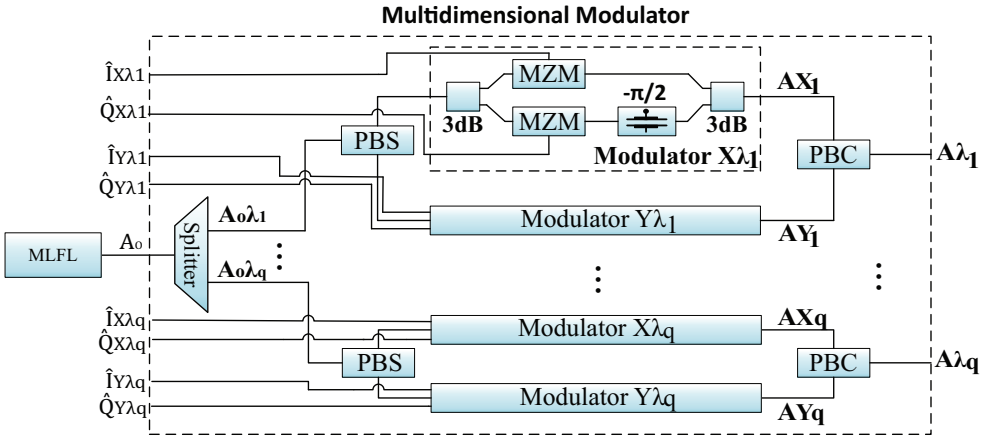

(c) Multidimensional modulator scheme

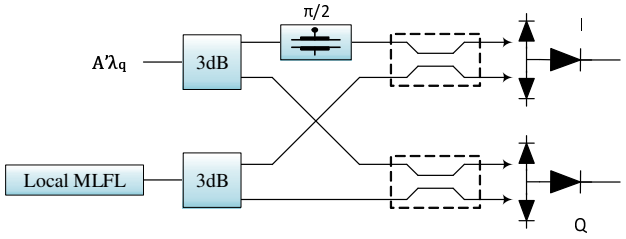

(d) Coherent Detector scheme

A: Optical Pulse.
H-APFDP: Hybrid-Amplitude Phase Frequency Dual Polarization.
M: Multidimensional Generator Matrix.
MLFL: Mode Locked Fiber Laser.
PBC: Polarization Beam Combiner.
PBS: Polarization Beam Splitter.

Fig. 3. H-SAPDP System.

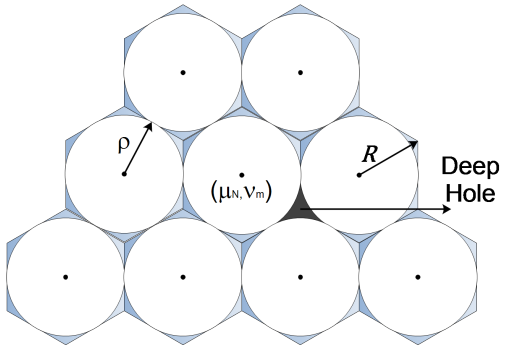

Fig. 4. Spherical Packing.

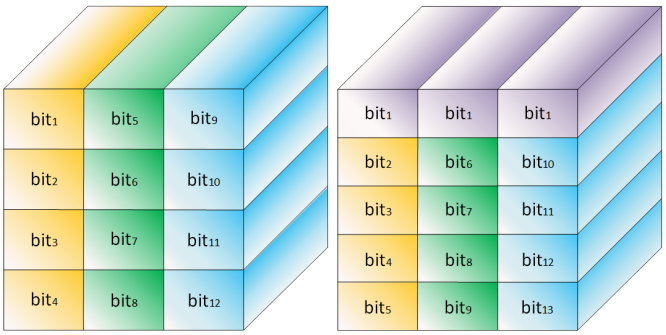

(a) 12-bit even alignment (b) 13-bit odd alignment

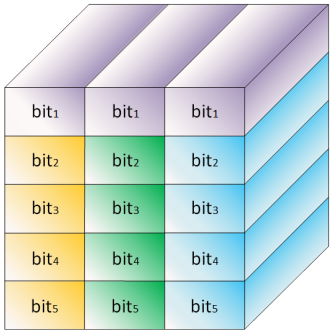

(c) 15-bit odd alignment

Fig. 5. Interleaver bit distribution.

E. Stokes and Polarized Signal Parameters

Based on the coherent properties of a light beam, the spin angular momentum defines the polarization state and the orbital angular momentum is associated with the azimuthal phase structure but is independent of the spin parameter. A geometric representation of the polarization state called the Jones vector was proposed in 1892; the amplitude and phase of the Jones Vector represent the 2D complex vectors of the electric field.

A_X and A_Y are used to denote the amplitudes of the waves in the two components of the electric field vector and their respective phases. The product between a Jones vector and a complex number gives a different Jones vector represented in the same state of polarization.

To represent the monochromatic Stokes parameters [20] as a linear expansion, we use the Jones vectors of the instantaneous electric field as elements of the coherency matrix of the ***n-th*** wave and combine them by Pauli matrices [23] as follows:

Any wave may be regarded as the sum of independent waves (completely unpolarized and completely polarized waves):

$$A_X = \sum_{n=1}^{N} {A_X}^{(n)}(t), \quad A_Y = \sum_{n=1}^{N} {A_Y}^{(n)}(t) \tag{11}$$

Next, the coherency matrix is written as the conjugate of each element in the matrix, which produces a ***Hermitian*** matrix:

$$\begin{aligned} J &= \begin{bmatrix} J_{XX} & J_{XY} \\ J_{YX} & J_{YY} \end{bmatrix} \\ &= \begin{bmatrix} < A_X A_X^* > & < A_X A_Y^* > \\ < A_Y A_X^* > & < A_Y A_Y^* > \end{bmatrix} \end{aligned} \tag{12}$$

The Stokes parameters are physically measurable and are properties represented as follows [24]:

$$\begin{aligned} \sigma_0 &= \begin{pmatrix} 1 & 0 \\ 0 & 1 \end{pmatrix}; \quad \sigma_1 = \begin{pmatrix} 1 & 0 \\ 0 & -1 \end{pmatrix} \\ \sigma_2 &= \begin{pmatrix} 0 & 1 \\ 1 & 0 \end{pmatrix}; \quad \sigma_3 = \begin{pmatrix} 0 & -j \\ j & 0 \end{pmatrix}. \end{aligned} \tag{13}$$

The coherency matrix is not easy to visualize, so we describe the partially polarized radiation in terms of the total beam intensity (S_0). S_1 and S_2 denote the azimuthal phase information for the right and left circular polarizations, respectively and S_3 is defined as [25]. Thus, the Stokes parameters can be written as functions of the intensity and polarization as follows:

$$\begin{aligned} S_0 &= (A_X^* A_Y^*) \begin{pmatrix} 1 & 0 \\ 0 & 1 \end{pmatrix}; \\ &= J_{XX} + J_{YY}; \\ &= A_X^2 + A_Y^2; \\ S_1 &= (A_X^* A_Y^*) \begin{pmatrix} 1 & 0 \\ 0 & -1 \end{pmatrix} \begin{pmatrix} A_X \\ A_Y \end{pmatrix}; \\ &= J_{XX} - J_{YY}; \\ &= A_X^2 - A_Y^2; \\ S_2 &= (A_X^* A_Y^*) \begin{pmatrix} 0 & 1 \\ 1 & 0 \end{pmatrix} \begin{pmatrix} A_X \\ A_Y \end{pmatrix}; \\ &= J_{XY} + J_{YX}; \\ &= 2 \cdot A_X \cdot A_Y \cdot Cos\,(\delta); \\ S_3 &= (A_X^* A_Y^*) \begin{pmatrix} 0 & -j \\ j & 0 \end{pmatrix} \begin{pmatrix} A_X \\ A_Y \end{pmatrix}; \\ &= j\,(J_{YX} - J_{XY}); \\ &= j\,(2 \cdot A_X \cdot A_Y \cdot Sin\,(\delta)); \\ \delta &= \theta_X - \theta_Y \end{aligned} \tag{14}$$

Neglecting the first Stokes parameter (S_0), the last three Stokes parameters can be plotted directly in a 3D coordinate system to generate the so-called Poincaré sphere [26], as shown in Fig. 6.

A normalized Stokes vector S' is obtained by dividing the Stokes vector by the total intensity (S_0). However, the partially polarized states lie inside the Poincaré sphere at a distance of

	S_0	S_1	S_2	S_3	A_X	A_Y	I_X	Q_X	I_Y	Q_Y
0000	$\sqrt{3}/2$	0	0	$\sqrt{3}/2$	$\sqrt{3}/4$	$\sqrt{3}/4$	$-1/2$	$-1/2$	$-1/2$	$-1/2$
0001	$\sqrt{3}/2$	0	$-\sqrt{3}/2$	0	$\sqrt{3}/4$	$-\sqrt{3}/4$	$-1/2$	$-1/2$	$-1/2$	$1/2$
0010	$\sqrt{3}/2$	0	$\sqrt{3}/2$	0	$\sqrt{3}/4$	$\sqrt{3}/4$	$-1/2$	$-1/2$	$1/2$	$-1/2$
0011	$\sqrt{3}/2$	0	0	$-\sqrt{3}/2$	$\sqrt{3}/4$	$-\sqrt{3}/4$	$-1/2$	$-1/2$	$1/2$	$1/2$
0100	$\sqrt{3}/2$	0	$\sqrt{3}/2$	0	$-\sqrt{3}/4$	$\sqrt{3}/4$	$-1/2$	$1/2$	$-1/2$	$-1/2$
0101	$\sqrt{3}/2$	0	0	$\sqrt{3}/2$	$-\sqrt{3}/4$	$-\sqrt{3}/4$	$-1/2$	$1/2$	$-1/2$	$1/2$
0110	$\sqrt{3}/2$	0	0	$-\sqrt{3}/2$	$-\sqrt{3}/4$	$\sqrt{3}/4$	$-1/2$	$1/2$	$1/2$	$-1/2$
0111	$\sqrt{3}/2$	0	$-\sqrt{3}/2$	0	$-\sqrt{3}/4$	$-\sqrt{3}/4$	$-1/2$	$1/2$	$1/2$	$1/2$
1000	$\sqrt{3}/2$	0	$-\sqrt{3}/2$	0	$-\sqrt{3}/4$	$\sqrt{3}/4$	$1/2$	$-1/2$	$-1/2$	$-1/2$
1001	$\sqrt{3}/2$	0	0	$-\sqrt{3}/2$	$-\sqrt{3}/4$	$-\sqrt{3}/4$	$1/2$	$-1/2$	$-1/2$	$1/2$
1010	$\sqrt{3}/2$	0	0	$\sqrt{3}/2$	$-\sqrt{3}/4$	$\sqrt{3}/4$	$1/2$	$-1/2$	$1/2$	$-1/2$
1011	$\sqrt{3}/2$	0	$\sqrt{3}/2$	0	$-\sqrt{3}/4$	$-\sqrt{3}/4$	$1/2$	$-1/2$	$1/2$	$1/2$
1100	$\sqrt{3}/2$	0	0	$-\sqrt{3}/2$	$\sqrt{3}/4$	$\sqrt{3}/4$	$1/2$	$1/2$	$-1/2$	$-1/2$
1101	$\sqrt{3}/2$	0	$\sqrt{3}/2$	0	$\sqrt{3}/4$	$-\sqrt{3}/4$	$1/2$	$1/2$	$-1/2$	$1/2$
1110	$\sqrt{3}/2$	0	$-\sqrt{3}/2$	0	$\sqrt{3}/4$	$\sqrt{3}/4$	$1/2$	$1/2$	$1/2$	$-1/2$
1111	$\sqrt{3}/2$	0	0	$\sqrt{3}/2$	$\sqrt{3}/4$	$-\sqrt{3}/4$	$1/2$	$1/2$	$1/2$	$1/2$

TABLE I
STOKES AND POLARIZED SIGNAL PARAMETERS FOR CUBIC LATTICE.

$P' = \sqrt{S_1'^2 + S_2'^2 + S_3'^2}$ from the origin. Thus, when the non-polarized component is not of interest, the Stokes vector can normalized as follows:

$$S'' = \frac{1}{P'} \begin{bmatrix} 1 \\ S_1' \\ S_2' \\ S_3' \end{bmatrix} \tag{15}$$

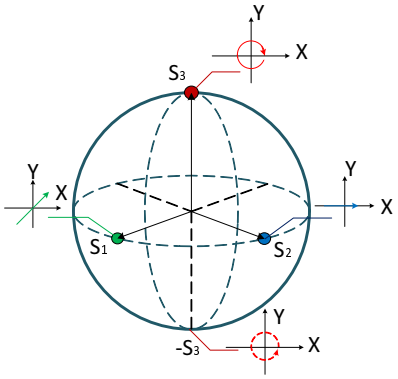

Fig. 6. Poincaré sphere.

Then, the outputs of the H-SAPDP transmitters are forwarded to a combiner before being transmitted via the optical fiber. On the receiver side, as shown in Fig. 3(b), the signal is split into λ_q branches, forwarded to the H-SAPDP receivers, and sampled at the symbol rate. The process of information recovery begins by using a PBS to separate the X - Y polarized information from $A'\lambda_q$ to retrieve the IQ signal through the coherent detector, as shown in Fig. 3(d).

All of the IQ polarized sub-carrier signals are forwarded by a digital equalizer in order to compensate the obtained signal removing the training symbols by applying the intra-symbol frequency-domain averaging channel estimation technique developed previously [27]. Next, demapping was applied to these signals to yield 16 or 32 multidimensional symbols placed in cubic or spherical lattices, respectively, as shown in Fig, 7 and Fig. 8, respectively, to form a hypercube or polyhedron, respectively. Based on the theory of molecular links, the use of these geometric figures can reduce the symbol energy due to grouping and allow more data to be transmitted. Then, the output signals are forwarded to deinterleaver and,

	S_0	S_1	S_2	S_3	A_X	A_Y	I_X	Q_X	I_Y	Q_Y
00000	$\sqrt{3}/2$	0	0	$\sqrt{3}/2$	$\sqrt{3}/4$	$\sqrt{3}/4$	$-\frac{1}{2}$	$-\frac{1}{2}$	$-\frac{1}{2}$	$-\frac{1}{2}$
00001	$\sqrt{3}/2$	0	$-\sqrt{3}/2$	0	$\sqrt{3}/4$	$-\sqrt{3}/4$	$-1/2$	$-1/2$	$-1/2$	$1/2$
00010	$\sqrt{3}/2$	0	$\sqrt{3}/2$	0	$\sqrt{3}/4$	$\sqrt{3}/4$	$-1/2$	$-1/2$	$1/2$	$-1/2$
00011	$\sqrt{3}/2$	0	0	$-\sqrt{3}/2$	$\sqrt{3}/4$	$-\sqrt{3}/4$	$-1/2$	$-1/2$	$1/2$	$1/2$
00100	$\sqrt{3}/2$	0	$\sqrt{3}/2$	0	$-\sqrt{3}/4$	$\sqrt{3}/4$	$-1/2$	$1/2$	$-1/2$	$-1/2$
00101	$\sqrt{3}/2$	0	0	$\sqrt{3}/2$	$-\sqrt{3}/4$	$-\sqrt{3}/4$	$-1/2$	$1/2$	$-1/2$	$1/2$
00110	$\sqrt{3}/2$	0	0	$-\sqrt{3}/2$	$-\sqrt{3}/4$	$\sqrt{3}/4$	$-1/2$	$1/2$	$1/2$	$-1/2$
00111	$\sqrt{3}/2$	0	$-\sqrt{3}/2$	0	$-\sqrt{3}/4$	$-\sqrt{3}/4$	$-1/2$	$1/2$	$1/2$	$1/2$
01000	$\sqrt{3}/2$	0	$-\sqrt{3}/2$	0	$-\sqrt{3}/4$	$\sqrt{3}/4$	$1/2$	$-1/2$	$-1/2$	$-1/2$
01001	$\sqrt{3}/2$	0	0	$-\sqrt{3}/2$	$-\sqrt{3}/4$	$-\sqrt{3}/4$	$1/2$	$-1/2$	$-1/2$	$1/2$
01010	$\sqrt{3}/2$	0	0	$\sqrt{3}/2$	$-\sqrt{3}/4$	$\sqrt{3}/4$	$1/2$	$-1/2$	$1/2$	$-1/2$
01011	$\sqrt{3}/2$	0	$\sqrt{3}/2$	0	$-\sqrt{3}/4$	$-\sqrt{3}/4$	$1/2$	$-1/2$	$1/2$	$1/2$
01100	$\sqrt{3}/2$	0	0	$-\sqrt{3}/2$	$\sqrt{3}/4$	$\sqrt{3}/4$	$1/2$	$1/2$	$-1/2$	$-1/2$
01101	$\sqrt{3}/2$	0	$\sqrt{3}/2$	0	$\sqrt{3}/4$	$-\sqrt{3}/4$	$1/2$	$1/2$	$-1/2$	$1/2$
01110	$\sqrt{3}/2$	0	$-\sqrt{3}/2$	0	$\sqrt{3}/4$	$\sqrt{3}/4$	$1/2$	$1/2$	$1/2$	$-1/2$
01111	$\sqrt{3}/2$	0	0	$\sqrt{3}/2$	$\sqrt{3}/4$	$-\sqrt{3}/4$	$1/2$	$1/2$	$1/2$	$1/2$
10000	1/4	$-1/4$	0	0	0	$-1/2$	0	0	0	-1
10001	1/4	$-1/4$	0	0	0	1/2	0	0	0	1
10010	1/4	$-1/4$	0	0	0	$-1/2$	0	0	-1	0
10011	1/4	$-1/4$	0	0	0	1/2	0	0	1	0
10100	1/4	1/4	0	0	1/2	0	0	-1	0	0
10101	1/4	1/4	0	0	$-1/2$	0	0	1	0	0
10110	1/4	1/4	0	0	1/2	0	-1	0	0	0
10111	1/4	1/4	0	0	$-1/2$	0	1	0	0	0
11000	1/2	0	1/4	0	1/2	1/2	-1	0	0	-1
11001	1/2	0	$-1/4$	0	1/2	$-1/2$	-1	0	0	1
11010	1/2	0	$-1/4$	0	$-1/2$	1/2	1	0	0	-1
11011	1/2	0	1/4	0	$-1/2$	$-1/2$	1	0	0	1
11100	1/2	0	$-1/4$	0	1/2	1/2	0	-1	-1	0
11101	1/2	0	1/4	0	1/2	$-1/2$	0	-1	1	0
11110	1/2	0	1/4	0	$-1/2$	1/2	0	1	-1	0
11111	1/2	0	$-1/4$	0	$-1/2$	$-1/2$	0	1	1	0

TABLE II
STOKES AND POLARIZED SIGNAL PARAMETERS FOR POLYHEDRAL LATTICE.

finally, to the bit log-likelihood ratio calculator which provide N LDPC decoders with the appropriate code rate, $[k/n]$. This process helps to improve the system performance (i.e., reduce the BER) without increasing the system's complexity.

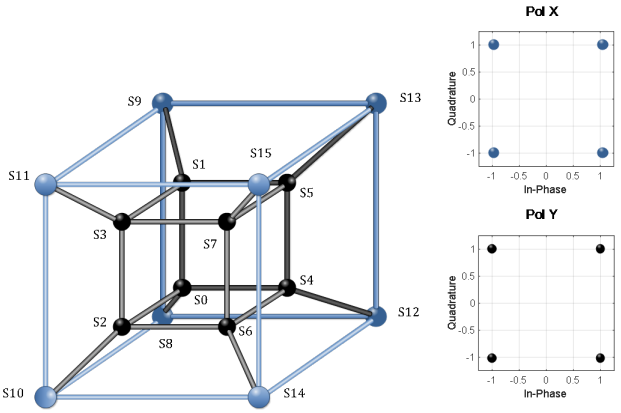

Fig. 7. Multidimensional Construction of the hypercube.

III. MULTIDIMENSIONAL SIMULATION SETUP AND NUMERICAL RESULTS

The functionality of the H-SAPDP LDPC-coded-modulation system was tested by simulation in MATLAB based on the parameters shown in Table III.

For the DP pulse propagation, the split-step Fourier method extension presented in [28] was used to present the Schrödinger propagation at the single-mode in the $X - Y$ plane.

In the first scenario, the BER performance was analyzed for 4D signal transmitted through each 4D sub-carrier $\lambda_1, \ldots, \lambda_q$, with 12 bits. The symbol data constellations were built according to polarized signal parameters as shown in Table I in

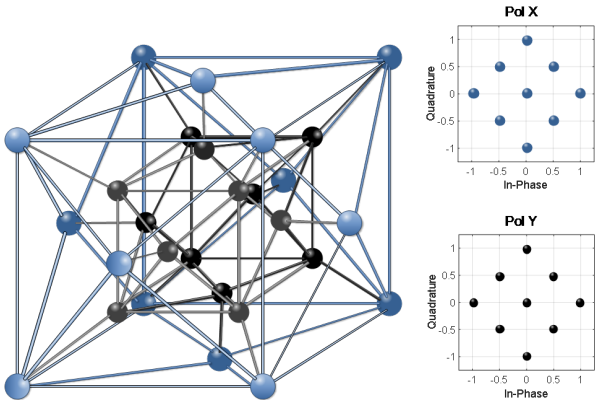

Fig. 8. Multidimensional Construction of the polyhedron.

	Value	Unit
Distance	$50/80/100$	$[Km]$
Attenuation (α)	0.18	$[dB/Km]$
Non-linearity Index (η_2)	$2.6e^{-20}$	$[m^2/W]$
A_{eff}	$80e^{-12}$	$[m^2]$
Dispersion Slope (S)	0.056	$[ps/\left(nm^2 \cdot Km\right)]$
Dispersion (D)	18	$[ps/\left(nm \cdot Km\right)]$
Sub-Wavelength (λ_n)	$1543/1548/1553$	$[nm]$
Carrier Frequency (f_c)	193.56	$[THz]$
Modulation Frequency (f_m)	50	$[GHz]$
Modulation Period (T_m)	20	$[ps]$
Initial Pulse Amplitude (A_0)	0.5	$[-]$
Carrier Period (T_s)	5.1667	$[fs]$
Sources	$[25 \times 1200]$	$[bits]$
LDPC Encoder	$[25 \times 2400]$	$[bits]$
Interleaver Cube	$[12 \times 5000]$	$[bits]$
Interleaver Polyhedron	$[15 \times 4616]$	$[bits]$
Bit Rate Cube	300	$[Gbps]$
Bit Rate Polyhedron	375	$[Gbps]$
Information Bits Cube	12	$[bits]$
Information Bits Polyhedron	13	$[bits]$

TABLE III
SIMULATION PARAMETERS.

order to represent the 16-points in 3D. Fig. 9(a) shows the results after transmission over distances of 50, 80, and 100 km. The best result was obtained over 50 km, exhibiting a very close response with an OSNR of 6dB and a $BER = 10^{-6}$. The transmission rate, defined as the product of the number of sub-carriers, the modulation frequency, the bits transmitted and codification rate $(3 \times 50 \times 4 \times 0.5)$, was 300 Gbps.

The performance in terms of BER was excellent compared to that achieved using traditional modulation techniques with 2D dimensions over a transmission distance of 100 km. Moreover, the proposed hybrid technique made it possible to transmit more information (up 256-QAM) while, at the same time, reducing the OSNR.

Fig. 10(a) shows the 4D constellation diagram mapped in 3D space for one sub-carrier. This was the expected result of the hypercube construction based on the molecular technique with identical inscribed polygons. The OSNR in the back-to-back configuration was set to 10 dB to visualize the multidimensional system noise.

The hypercube was generated by setting the height and length in the first two dimensions based on the I_Y/Q_Y data, the width in third-dimension was set based on the Q_X data, and an internal or external cube was selected (i.e., the fourth dimension based on the I_X data. In this way, the 4D symbol generates the lattice despite the noise to facilitate suitable robust transmission.

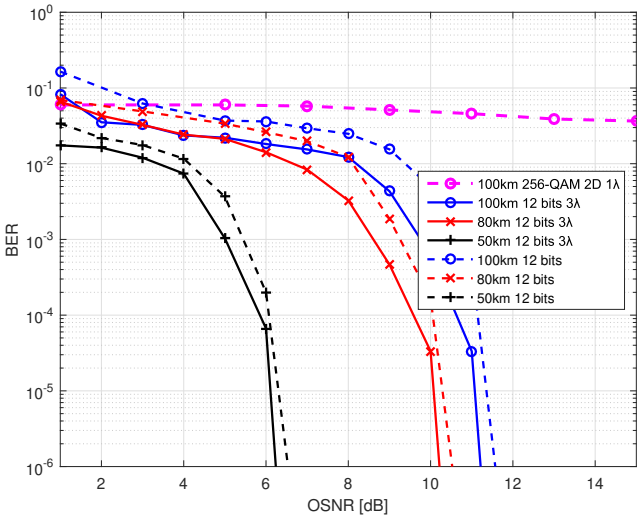

(a) BER performance with a 4D cubic lattice (even alignment)

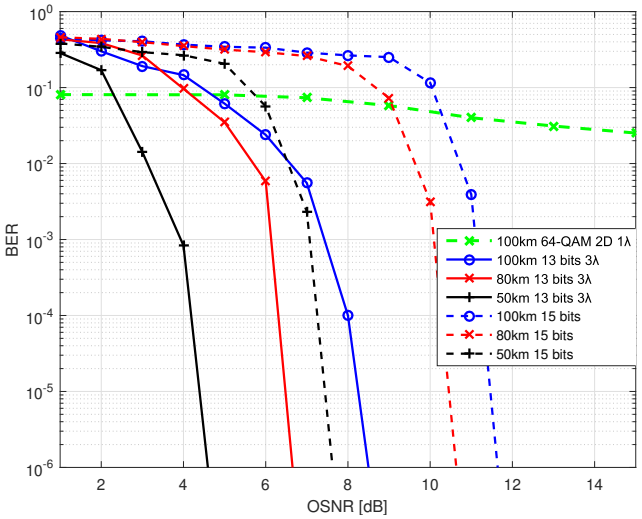

(b) BER performance with a polyhedral lattice (odd alignment)

Fig. 9. BER performance analysis

Similarly, Fig. 9(b) shows the BER performance when an odd alignment was used to generate a 4D polyhedron constellation for each sub-carrier.

With the polyhedron technique, a gain of 2dB of gain in terms of the OSNR was achieved for 12 bit transmission over 50 km while transmission over 80 and 100 km resulted in a 3 dB OSNR gain. Furthermore, the BER was approximately 10^{-6} for 12 bit transmission. In this context, it is more convenient to work with an additional bit but the same performance cannot be achieved with 15 bits due to the packing process.

As, the multidimensional system noise sensibility for the 4D-polyhedron constellation is presented in Fig. 10(b) shows the result when a back-to-back configuration is used again, the OSNR was set at 10 dB to visualize the hypercube and polyhedron techniques under the same conditions.

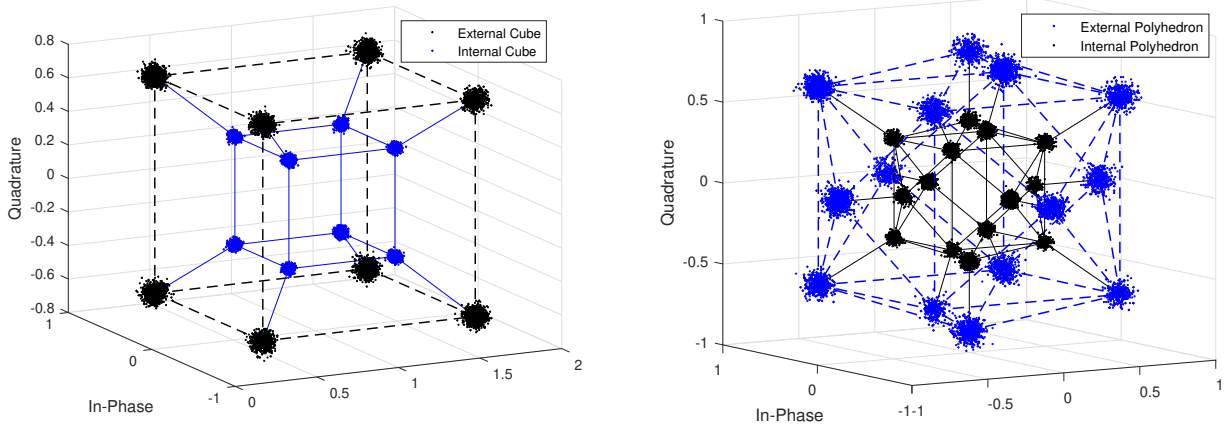

(a) Back-to-back representation of the 4D cubic lattice (even alignment) with an OSNR of 10 dB.

(b) Back-to-back representation of the 4D polyhedral lattice (odd alignment) with an OSNR of 10 dB.

Fig. 10. 4D Geometric Shapes

In the non-linear effect, the spectral envelope gives rise to a wider peak power due to chromatic dispersion and non-linear phase variation on X-Y plane; this effect generates new optical frequency components as the pulses propagates.

It is important to note that this non-linearity effect is due to transmission distance and the wavelength compression due to data packing for single-channel transmission. In this system, increasing the wavelength could cause a distortion in the system and, consequently, degraded the SE. However with three sub-carriers the SE and BER are very stable over long distances, as shown in Fig. 12 and Fig. 13. Note that the effect of wave mixing occurs when N-subcarriers are used. However it is not necessary to analyze the non-linearity or implement compensation to avoid channel interference, for the reasons described previously.

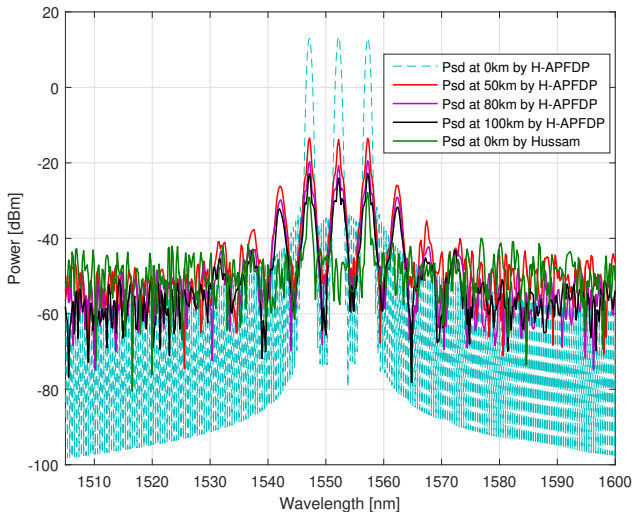

Fig. 11. PSD with the proposed system at an OSNR of 5 dB.

Spectral density (PSD) was obtained using Equation (16), where Ts is the period for a pulse and $R(k)$ represents the pulse auto correlation defined in Equation (17) for a bipolar

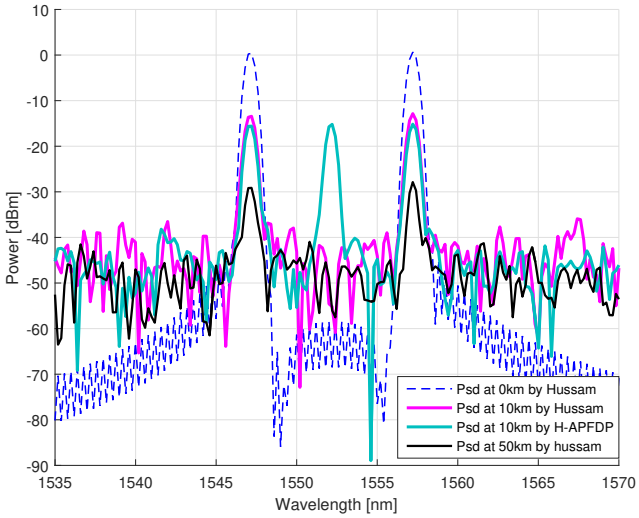

Fig. 12. Comparison of the PSD with an OSNR of 5 dB.

RZ signal.

$$\mathscr{P}(f) = \frac{\left|\mathscr{F}\left\{A_{OUT}(t)\right\}\right|^2}{T_s} \sum_{k=-\infty}^{\infty} R(k)\, e^{jk2\pi f_c t T_s} \tag{16}$$

$$R(k) = \left\{ \begin{array}{cc} \frac{|A_{out}|^2}{2} & k = 0 \\ \frac{-|A_{out}|^2}{4} & |k| = 1 \\ 0 & |k| > 1 \end{array} \right\} \tag{17}$$

Given the complex envelopment signal, A_{OUT}, the PSD function in Equation (16) can b rewritten as follows

$$\begin{aligned} \mathscr{P}(f) &= \frac{|A_{OUT}(t)|^2 T_s}{8} \left(\frac{Sin(\pi t T_s/2)}{\pi t T_s/2}\right)^2 (1 - Cos(2\pi f_c T_s)) \\ \mathscr{P}(f) &= \frac{|A_{OUT}(t)|^2 T_s}{4} \left(\frac{Sin(\pi t T_s/2)}{\pi t T_s/2}\right)^2 \left(Sin^2(\pi f_c T_s)\right) \end{aligned} \tag{18}$$

The PSD in Fig. 11 show that two new frequency components occurred at 1542 and 1562 nm due to chromatic dispersion over the propagation distance. This secondary frequency

has 13.66% of less power than the central pulse peak power at a transmission distance of 50 km.

Hussam system, which only supports transmission over a distance of 10 km using two sub-carriers, is compared with the proposed system in terms of PSD in Fig. 12. Comparing the PSDs of the H-SAPDP with those of the Hussam system the insertion of one additional sub-carrier degraded the SE but the H-SAPDP remained superior compared to the Hussam system at equal and greater distances.

We further compare the proposed system with the Poincaré technique developed by Hussam. The Poincare technique one of the most promising multidimensional modulation techniques for double polarization in 3D space. It involves the use of a dodecahedral geometry for symbol mapping. It achieves impressive results in back-to-back transmission. However, the Poincaré technique cannot be supported beyond 10 km of distance while, in contrast, we demonstrated that the distance does not impede transmission by our system at different wavelengths. We neglect the case of interleaved bit distribution with 15-bit alignment because of its poor performance in terms of the BER. Fig 13 shows the comparison of the BER performance of these two techniques. In this context, the best result was obtained over a distance of 10 km with the 13-bit format and the polyhedral technique at an OSNR of 3 dB: this method provided 1 dB of gain compared to the Poincaré sphere. The benefits of the proposed system become more pronounced at greater distances such as 50 km or more.

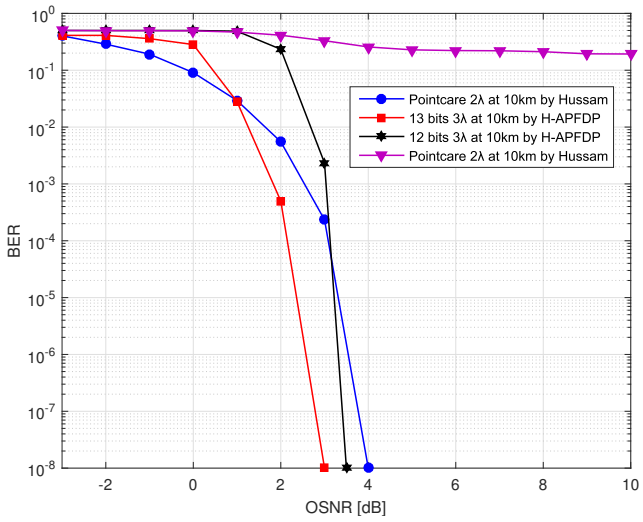

Fig. 13. Comparison of BER Performance.

Also, in order to achieve a beyond 1Tb/s transmission, our proposed is evaluated over optical time division multiplexing (OTDM), based on Nyquist filter combined by MLFL to generate a Nyquist pulse train [29]. In the reception, a homodyne coherent detection presented in [30] achieves 1.2Tb/s transmission for 12 bit system and 1.5Tb/s for the 13 bits system using 4-time slots.

The simulation results, expressed at Fig. 14, shows the power reduction over the OTDM transmitted signal. We can compare with the Fig. 12, where the system is widely affected when is used OTDM signal, having a penalty of 12dB with

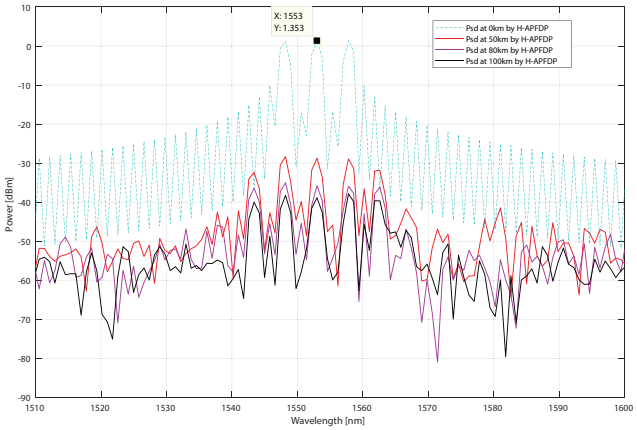

Fig. 14. PSD with the proposed system using 4 channels OTDM at an OSNR of 5 dB.

respect to non-OTDM signal. This reduction of peak to average in OTDM signal is due to Nyquist pulse compression [31]. Consequently the SE is degraded even more if the distance is increased. Concluding in this way, that there exist a trade-off between the transmission rate and the Spectral Efficiency due to the time-multiplexing degrades being this very important penalty to consider when implementing complex high-speed systems.

IV. Conclusions

In this study, we demonstrated that the novel H-SAPDP LDPC-coded-modulation system can improve the BER performance for long-distance transmission. In addition we demonstrated a novel technique based on the Poincaré sphere and Stokes parameters to achieve more data packaging in the 3D space. The results are promising since multidimensional modulation can achieve transmission with similarities to both high-index traditional modulation in that the SE is excellent and low-index traditional modulation in that the BER is greatly improved.

Moreover, we implemented the Pol-Mux technique in a WDM environment using three sub-carriers to achieve $12-bit$ even alignment transmission, which is not possible with other types of 4D independent carrier modulation. We further expanded the technique to be N-dimensional for handling 13 and 15 bits by adding an additional bit for each wavelength. Cubic and polyhedral signal constellations were used to improve the BER performance to 3 dB for the odd configuration and 0.3 dB for the even configuration.

From a system general performance perspective, 13-bits odd configuration offers more robust transmission compare to a simple 4D transmission over a single-mode fiber.

Finally, the simulation over a transmission distance of 100 Km indicates that, when using the multidimensional matrix; to package the mapping information, the 13-bit odd dual lattice provides better performance the even dual lattice in 2.7 dB with a $BER = 10^{-6}$.

In future studies, the SE can be improved further by analyzing the non-linear channel formed due to the increased number of sub-carriers. Moreover, to apply new techniques of

compensating for the four-wave-mixing effects, the number of lambdas should be increased in future iterations of the system.

References

[1] G. D. Forney and L. F. Wei, "Multidimensional Constellations-Part I: Introduction. Figures of Merit, and Generalized Cross Constellations," *IEEE Journal on Selected Areas in Communications*, vol. 7, no. 6, pp. 877–892, 1989.

[2] M. Taherzadeh, H. Nikopour, A. Bayesteh, and H. Baligh, "SCMA Codebook Design." Vancouver, BC, Canada: Vehicular Technology Conference (VTC Fall), 2014 IEEE 80th, 2014.

[3] S. G. Evangelides, L. F. Mollenauer, J. P. Gordon, and N. S. Bergano, "Polarization Multiplexing with Solitons," *Journal of Lightwave Technology*, vol. 10, no. 1, pp. 28–35, 1992.

[4] D. Qian, N. Cvijetic, J. Hu, and T. Wang, "108 Gb/s OFDMA-PON With Polarization Multiplexing and Direct Detection," *Journal of Lightwave Technology*, vol. 28, no. 4, pp. 484–493, 2010.

[5] F. Tian, D. Guo, B. Liu, Q. Zhang, Q. Tian, R. Ullah, and X. Xin, "A novel concatenated coded modulation based on gfdm for access optical networks," *IEEE Photonics Journal*, vol. 10, no. 2, pp. 1–8, 2018.

[6] H. G. Batshon, I. B. Djordjevic, L. L. Minkov, L. Xu, T. Wang, and M. Cvijetic, "Proposal to Achieve 1 Tb/s per Wavelength Transmission Using Three-Dimensional LDPC-Coded Modulation," *IEEE Photonics Technology Letters*, vol. 20, no. 9, pp. 721–723, 2008.

[7] S. O. Arik, D. Millar, T. Koike-Akino, K. Kojima, and K. Parsons, "High-dimensional modulation for mode-division multiplexing," in *Optical Fiber Communication Conference*. Optical Society of America, 2014, pp. W4J–1.

[8] H. Bülow, "Polarization QAM modulation (POL-QAM) for coherent detection schemes," *Optical Fiber Communication Conference*, no. OWG2, pp. 25–27, 2009.

[9] J. K. Fischer, C. Schmidt-Langhorst, S. Alreesh, R. Elschner, F. Frey, P. W. Berenguer, L. Molle, M. Nölle, and C. Schubert, "Generation, transmission, and detection of 4-d set-partitioning qam signals," *Journal of Lightwave Technology*, vol. 33, no. 7, pp. 1445–1451.

[10] M. Arabaci, I. B. Djordjevic, L. Xu, and T. Wang, "Four-dimensional nonbinary LDPC-coded modulation schemes for ultra-high-speed optical fiber communication," *IEEE Photonics Technology Letters*, vol. 23, no. 18, pp. 1280–1282, 2011.

[11] J. Leibrich and W. Rosenkranz, "Power efficient multidimensional constellations," pp. 1–6, 2014.

[12] H. G. Batshon and I. B. Djordjevic, "Beyond 240 gb/s per wavelength optical transmission using coded hybrid subcarrier/amplitude/phase/polarization modulation," *IEEE Photonics Technology Letters*, vol. 22, no. 5, pp. 299–301, 2010.

[13] ——, "Hybrid amplitude/phase/polarization coded modulation for 100 gb/s optical transmission and beyond," in *LEOS Annual Meeting Conference Proceedings, 2009. LEOS'09. IEEE*. IEEE, 2009, pp. 644–645.

[14] N. S. J.H Conway, *Sphere Packings, Lattices and Groups*, 1998, vol. 338.

[15] F. Buchali and H. Bülow, "Experimental transmission with polqam and ps-qpsk modulation format using a 28-gbaud 4-d transmitter," pp. We–3, 2012.

[16] H. G. Batshon, I. Djordjevic, and T. Schmidt, "Ultra high speed optical transmission using subcarrier-multiplexed four-dimensional LDPC-coded modulation," *Opt. Express*, vol. 18, no. 19, pp. 20 546 – 20 551, 2010.

[17] J. Yao, J. Yao, Y. Wang, S. C. Tjin, Y. Zhou, Y. Loy Lam, J. Liu, and C. Lu, "Active mode locking of tunable multi-wavelength fiber ring laser," *Optics Communications*, vol. 191, no. 3-6, pp. 341–345, 2001.

[18] D. T. Nguyen, J. Abou, and A. Morimoto, "Ultrashort pulse generation using fiber FM laser," *Optical review*, vol. 19, no. 5, pp. 337 – 340, 2012.

[19] E. Agrell and M. Karlsson, "Power-Efficient Modulation Formats in Coherent Transmission Systems," *Journal of Lightwave Technology*, vol. 27, no. 22, pp. 5115 – 5126, 2009.

[20] M. Born and E. Wolf, "Principles of optics, chap. 1," *Cambridge University Press*, vol. 7, pp. 360–370, 1975.

[21] J. Renaudier, O. Bertran-Pardo, A. Ghazisaeidi, P. Tran, H. Mardoyan, P. Brindel, A. Voicila, G. Charlet, and S. Bigo, "Experimental Transmission of Nyquist Pulse Shaped 4-D Coded Modulation using Dual Polarization 16QAM Set-Partitioning Schemes at 28 Gbaud," *Optical Fiber Communication Conference/National Fiber Optic Engineers Conference 2013*, p. OTu3B.1, 2013.

[22] F. Buchali and H. Bülow, "Experimental transmission with POLQAM and PS-QPSK modulation format using a 28-Gbaud 4-D transmitter," in *Optical Communications (ECOC), 2012 38th European Conference and Exhibition on*. IEEE, 2012, pp. 1 – 3.

[23] J. Gil, "Polarimetric characterization of light and media," *Eur. Phys. J. Appl. Phys*, vol. 40, pp. 1–47, 2007.

[24] W. H. McMaster, "Matrix representation of polarization," *Reviews of modern physics*, vol. 33, no. 1, p. 8, 1961.

[25] G. Milione, H. Sztul, D. Nolan, and R. Alfano, "Higher-order poincaré sphere, stokes parameters, and the angular momentum of light," *Physical review letters*, vol. 107, no. 5, p. 053601, 2011.

[26] M. J. Padgett and J. Courtial, "Poincaré-sphere equivalent for light beams containing orbital angular momentum," *Optics letters*, vol. 24, no. 7, pp. 430–432, 1999.

[27] X. Liu and F. Buchali, "Intra-symbol frequency-domain averaging based channel estimation for coherent optical OFDM," *Optics Express*, vol. 16, no. 26, p. 21944, 2008.

[28] R. Deiterding and S. W. Poole, "Robust split-step Fourier methods for simulating the propagation of ultra-short pulses in single-and two-mode optical communication fibers," in *Splitting Methods in Communication, Imaging, Science, and Engineering*. Springer, 2016, pp. 603 – 625.

[29] M. Yoshida, J. Nitta, K. Kimura, K. Kasai, T. Hirooka, and M. Nakazawa, "Single-channel 3.84 Tbit/s, 64 QAM coherent Nyquist pulse transmission over 150 km with frequency-stabilized and mode-locked laser," in *Optical Fiber Communications Conference and Exhibition (OFC), 2017*. IEEE, 2017, pp. 1 – 3.

[30] N. D. Nguyen and L. N. Binh, "Demultiplexing techniques of 320 Gb/s OTDM-DQPSK signals: A comparison by simulation," in *Communication Systems (ICCS), 2010 IEEE International Conference on*. IEEE, 2010, pp. 171 – 175.

[31] R. Schmogrow, M. Winter, M. Meyer, D. Hillerkuss, S. Wolf, B. Baeuerle, A. Ludwig, B. Nebendahl, S. Ben-Ezra, J. Meyer *et al.*, "Real-time nyquist pulse generation beyond 100 gbit/s and its relation to ofdm," *Optics Express*, vol. 20, no. 1, pp. 317–337, 2012.